Applied Clay Science 134 (2016) 221–234

Contents lists available at ScienceDirect

Applied Clay Science

journal homepage: www.elsevier.com/locate/clay

Research paper

Illitization sequence controlled by temperature in volcanic geothermal systems: The Tinguiririca geothermal field, Andean Cordillera, Central Chile

Mercedes Vazquez [a,1], Blanca Bauluz [b,*], Fernando Nieto [c], Diego Morata [a]

[a] Department of Geology, Andean Geothermal Center of Excellence (CEGA), Facultad de Ciencias Físicas y Matemáticas, Universidad de Chile, Plaza Ercilla 803, Santiago, Chile
[b] Department of Earth Sciences, Universidad de Zaragoza, Pedro Cerbuna 12, Zaragoza, Spain
[c] Department of Mineralogy and Petrology, Andalusian Institute of Earth Sciences, Universidad de Granada-CSIC, Fuente Nueva s/n, Granada, Spain

ARTICLE INFO

Article history:
Received 23 November 2015
Received in revised form 30 March 2016
Accepted 9 April 2016
Available online 7 May 2016

Keywords:
Illite/smectite
XRD
HRTEM
Active geothermal systems
Andes

ABSTRACT

In this research, we have investigated the illitization process in Quaternary calc-alkaline volcanic and volcaniclastic rocks in the active Tinguiririca geothermal field (Andean Cordillera, central Chile). XRD, SEM, and HRTEM/AEM techniques have been used to establish the illitization sequence and evaluate the influence of the factors controlling the mineral reaction and kinetics at low temperature (T). Analysed samples were collected through a slimhole core up to 815 m deep in which the T was measured in situ (up to 230 °C at the bottom of the drill core). Textural information indicates that the dioctahedral clays have replaced most of the vitreous components. In contrast, plagioclase phenocrysts have only been partially and patchily albitized. The observed replacements imply dissolution-crystallization processes. The illitization sequence detected by XRD is apparently continuous from smectite to R3 I-S through R0 and R1, with a progressive increase in illite layers. HRTEM data show a similar illitization trend. However, the high-resolution images reveal that the clays are more heterogeneous than the XRD patterns suggest, with the coexistence of different types of dioctahedral clays at the sample level. They also indicate that the most abundant dioctahedral clays are smectite, R1 I-S, and illite. Therefore, the XRD patterns are probably the result of a mixture of these phases plus accessory I-S mixed layers with higher ordering ($R > 1$). Increasing T with depth would enhance the kinetic conditions necessary for illitization and also favour the dissolution of the vitreous K-rich component and, locally the albitization of plagioclases. Both processes release K, which, with the concomitant increase in T and K availability, enhances the crystallization of clays progressively richer in K. Thus, at T ≤ 85 °C smectite crystallizes, at ***T*** > 85 °C the conditions are appropriate for the crystallization of R1 I-S (with minor smectite + R0 I-S), up to T ≥ 175 °C, where illite is the most abundant and relatively stable phase.

1. Introduction

The sequential smectite-to-illite reaction via mixed-layer minerals (I-S) has been documented in low-temperature environments and is commonly associated with burial diagenesis and hydrothermal alteration. Most illitization studies report that, as I-S interstratified clays become illitic, the interlayer arrangements change from random (R0) to short-range (R1) ordered, and then to long-range (R3) ordered, where R is the Reichweite parameter (Jagodzinski, 1949).

There are many studies on the illitization process, although there are disagreements on the smectite-to-illite reaction model. Classically, smectite illitization in sedimentary basins has most often been described as a progressive illitization of smectite crystals (Weaver, 1960; Perry and Hower, 1970, 1972; Hower et al., 1976, among others). In contrast, sequences formed by discrete phases, such as smectite, R1 I-S, and illite, have been described in hydrothermal systems (e.g. Dong et al., 1997, Tillick et al., 2001; Yan et al., 2001; Bauluz et al., 2002; Inoue et al., 2004, 2005; Murakami et al., 2005, among others). These observations suggest that the illitization mechanism may be multiple, and two main types of transformation have therefore been proposed (Altaner and Ylagan, 1997): (1) solid-state transformation (e.g. Hower et al., 1976; Bell, 1986; Inoue et al., 1990; Amouric and Olives, 1991; Lindgreen et al., 1991; Baronnet, 1992; Drits et al., 1997; Cuadros and Altaner, 1998a, 1998b, among others) and (2) dissolution and crystallization (e.g. Ahn and Peacor, 1986; Inoue et al., 1987, 2004, 2005; Yau et al., 1987; Eberl and Srodon, 1988; Dong et al., 1997; Tillick et al., 2001; Yan et al., 2001; Bauluz et al., 2002; Murakami et al., 2005; Arostegui et al., 2006; Ferrage et al., 2011; Nadeau et al., 1984, 1985, among others). Regardless of the proposed mechanism for smectite

* Corresponding author.
E-mail address: bauluz@unizar.es (B. Bauluz).
[1] Present address: Departamento de Didáctica de Ciencias Experimentales, Universidad de Granada, Campus Universitario de Ceuta, Calle Cortadura del Valle, s/n, Ceuta, Spain.

http://dx.doi.org/10.1016/j.clay.2016.04.011
0169-1317/

illitization, there is agreement that this transformation and the crystal chemistry of mixed-layer I-S depend on T, compositions of fluid, time, and fluid/rock ratio during the formation of I-S minerals as well as the chemical composition of the precursor materials (Altaner and Ylagan, 1997).

Improvements in our knowledge of the smectite-to-illite reaction are important to understand the thermal evolution and maturity of sedimentary basins and the thermal history of rocks in active and fossil geothermal fields. Harvey and Browne (1991) observed two main mixed-layer clay mineral transformations in the Wairakei active geothermal system (New Zealand): the smectite to chlorite and the smectite to illite transformations. Clay minerals are usually developed in the shallower zone of active geothermal systems (Reyes, 1990). Kaolinite, dickite and pyrophyllite can be developed under acid conditions above upflow zones or from acid alteration within the reservoir. On the other hand, smectites, chlorite and illite crystallize under neutral pH conditions developing the clay cap zone that usually limits the geothermal reservoir, characterized by a propyllitic alteration, where trioctahedral chlorite is associated with variable amounts of epidote, quartz and other Ca-silicates (e.g. Mas et al., 2006, between others). Because the difference in conductivity between the clay-rich alteration zone reservoir domains, the evolution from the clay cap to the propyllitic zone could identified during the exploration phase in active geothermal systems by means of geophysical survey, in particular analysing the resistivity data. For this reason, the analysis of clay minerals in drill core in active geothermal systems is one of the more useful tools in any geothermal exploration program aimed to understand geothermal systems in depth. Consequently clay minerals study allow to constraint temperature and fluid evolution during hydrothermal alteration and also the control of primary rock on the fluid-flow during alteration. Moreover, hydrothermal alteration in active geothermal systems took place over a relatively short period of time and under variable fluid/rock ratio (e.g. Harvey and Browne, 1991; Inoue et al., 2004). Under these borderline constraints, smectite to illite transition in geothermal systems seems to be mostly controlled by temperature but also composition of precursor materials could improve the illite formation. In this sense, Harvey and Browne (1991) postulated about the strong control of permeability and fluid-flow on the nature and sequence of clay minerals in active geothermal systems. On the other hand, Ji and Browne (2000) concluded that illite crystallinity in active geothermal fields is strongly controlled by T, but lithology, potassium availability, and permeability also seem to be important controls on illite formation. Inoue et al. (2004) studied I/S series during geothermal alteration in felsic vitric volcaniclastic units and indicated the influence of the fluid/rock ratio and fluid geochemistry (pH and Na-rich solutions) in the illitization processes under geothermal conditions. According to these authors, smectite illitization obeys Ostwald's step rule as being a kinetically controlled transformation. Additionally, knowledge of the illitization sequence has also contributed to better understanding of how fault propagation occurs in crustal fault zones and in subduction regions (e.g. Deng and Underwood, 2001; Dubacq et al., 2010). In summary, different parameters seems to be controlling the smectite to illite transformation, and the possibility to analyse a continuous drill core from an active geothermal field is an unique opportunity for revealing new hypothesis about this type of mixed-layer evolution.

The study of the smectite-to-illite transformation in active geothermal systems using samples from a continuous drillhole is a unique opportunity to better understand this mineral transformation under a high (and known) geothermal gradient. In this paper, the illitization process has been investigated in the Tinguiririca geothermal field (Andean Cordillera of central Chile) combining X-ray diffraction (XRD), Scanning electron microscopy (SEM) and High resolution transmission electron microscopy (HRTEM) analyses in order to establish the illitization sequence and evaluate the influence of the different factors controlling the mineral reaction and the kinetics at low T. Vázquez et al. (2014) describe in this field the smectite-to-illite reaction as being a consequence of the hydrothermal alteration of volcanic rocks. In order to thoroughly investigate the illitization sequence, more detailed sampling was performed in the transition from the smectite to illite zones, and HRTEM techniques have been used to distinguish the interlayer order of smectite and illite layers and establish the sequence and the mechanism of illitization. Our new results inform the illitization processes and the different mechanisms that could be involved.

2. Geological setting

Andean geothermal systems are mostly related with the volcanism generated as a consequence of the subduction of the Nazca Plate under the South America Plate. In the Chilean Andean Cordillera, over seventy different geothermal fields are currently in the exploration stage by different private companies, and exploration drilling has been performed in nine of these areas (Lahsen et al., 2015). The Tinguiririca geothermal field, 150 km south-west of Santiago (central Chile), belongs to the Chilean Andean volcanic arc. Surficial geothermal expressions in the area (stem vents, bubbling mud pools, and flowing hot springs) are directly associated with the Tinguiririca Volcanic Complex (Clavero et al., 2011). Recent volcanic activity in this complex (<1.1 Ma; Arcos et al., 1988) has generated three main volcanic cones (Tinguiririca, Fray Carlos, and Montserrat) and several minor scoria cones, with the most recent historic eruption at the beginning of the last century (Arcos et al., 1988). The NNE alignment of these eruptive centres coincides with the main NNE fault system observed in the area (Fig. 1), suggesting a strong structural control both on the magmatic and also on the fluid-flow paths in this section of the Chilean Andes. Moreover, recent passive seismic tomography data (Pavez et al., 2016) corroborate the primary role of this NNE fault system in the mobility of hydrothermal fluids. The main surface thermal manifestations occur west and southwest of the Tinguiririca volcano (Fig. 1). Water and gas geochemistry sampled on surface together with He isotope ratios suggest equilibrium temperatures in between 230 and >300 °C having a clear magmatic source, possibly of basaltic composition (Clavero et al., 2011) related with active volcanoes of the Tinguiririca Volcanic Complex.

In the summer of 2011, the first slimhole well (Pte-1) was drilled on the southwestern flank of the Tinguiririca Complex, allowing the collection of altered rocks up to 813 m in depth. The borehole location by Energia Andina company was based on geological and geophysical (aeromagnetic, gravity and MT) survey previously done by this company. Temperatures measured directly in the borehole indicate a high thermal gradient at shallow depth (with a T close to 200 °C at a depth of 450 m). This drillhole intersects Holocene–Pleistocene volcanic and volcanoclastic rocks (calc-alkaline porphyritic basaltic to andesitic lava flows with minor pyroclastic levels) related to the volcanism of the Tinguiririca Volcanic Complex (Clavero et al., 2011, Droguett et al., 2012). The volcanic rocks are composed primarily of calcic plagioclase, clino and orthopyroxene, and minor olivine and magnetite phenocrysts within an intersertal to hyalopilitic groundmass (Droguett et al., 2012). Available whole-rock chemical data indicate a rather geochemical homogeneity of the mafic lavas of the Tinguiririca Volcanic Complex, with SiO_2 values ranging from 56 to 61 wt% and K_2O in the 3–5 wt% range (Arcos et al., 1988; Polanco et al., 2015), typical for calc-alkaline Andean andesites and basaltic andesites.

In previous studies of samples from Pte-1 borehole, Droguett et al. (2012) and Vázquez et al. (2014) described the alteration mineralogy of the hydrothermal systems of the Tinguiririca as T-dependent. Droguett et al. (2012) reported smectite and hematites to be the index minerals of a shallow alteration zone. This hydrothermal assemblage was considered an indicator of the so-called argillic alteration (from 0 to 410 m and 30 to 200 °C). These authors also identified epidote and prehnite at the deepest levels (from 600 to 813 m and 200 to 250 °C), developing a propylitic alteration consistent with almost neutral pH fluid conditions. Hydrothermal minerals fill open spaces (voids and

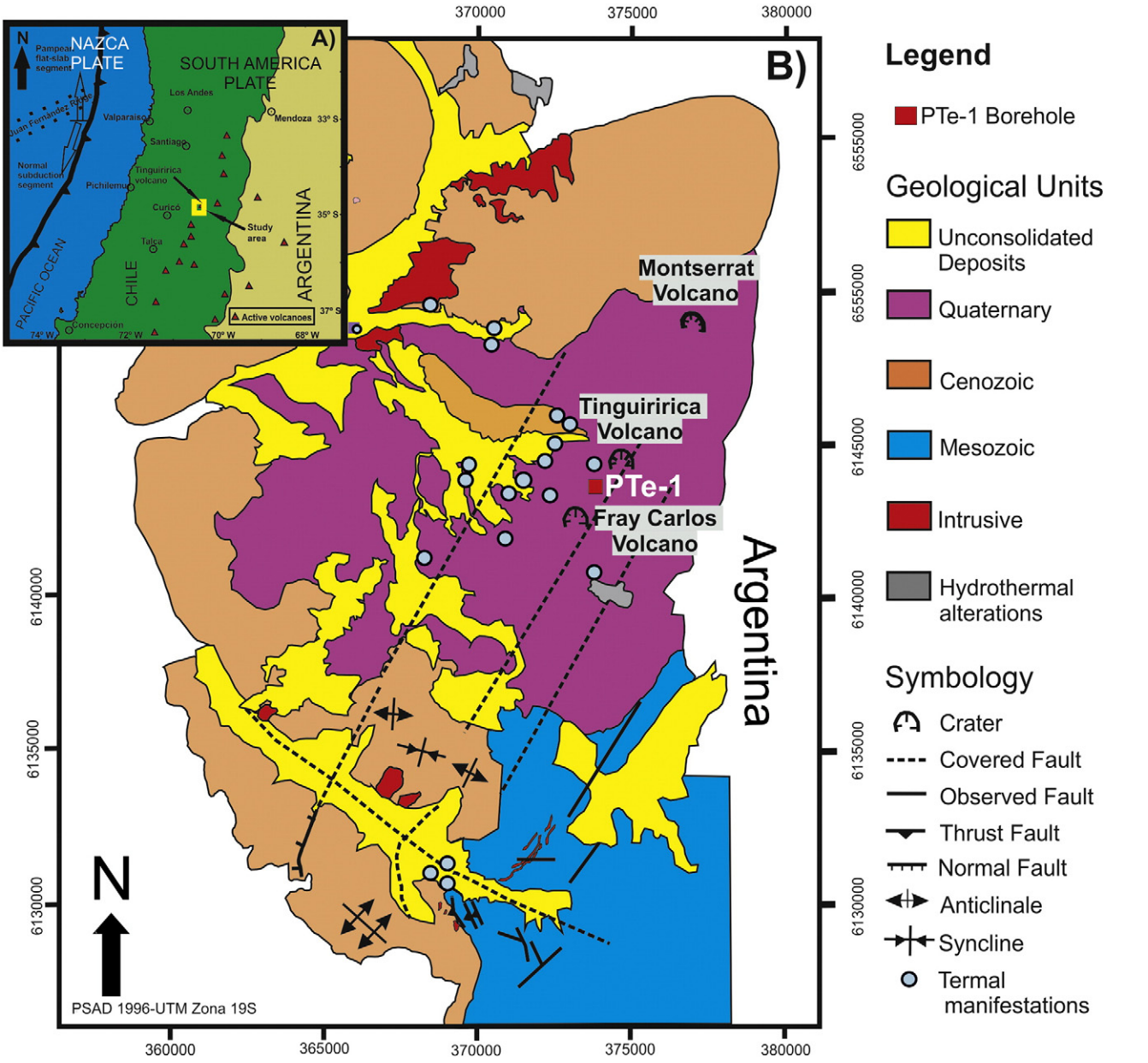

Fig. 1. Geological map of the Tinguiririca geothermal field, showing the location of thermal surface manifestations, the hydrothermal alteration areas, and the location of the PTE-1 drill core, simplified from Clavero et al. (2011).

fractures) and also replace most of the primary rock-forming minerals (mainly plagioclase and pyroxenes). Vázquez et al. (2014) distinguished four alteration zones in the hydrothermal systems of the Tinguiririca: (1) a shallow alteration zone dominated by smectite (from 0 to 300 m and 30 to 100 °C); (2) an R1 I-S mixed layer zone characterized by illitic-rich I-S mixed layers, high-charge corrensite, and chlorite (from 262 to 410 m and 100–180 °C); (3) an R3 I-S mixed-layer zone with illite-rich I-S mixed layers, together with chlorite and high-charge corrensite (from 410 to 700 m and 200–220 °C); and (4) a deep alteration zone, where chlorite and low-charge corrensite are the main clay minerals, and I-S mixed layers are absent (from 700 to the bottom of the drillhole and from 220 to 250 °C).

3. Materials and methods

With the aim of analysing the illitization processes, six samples were selected along borehole Pte-1 of the Tinguiririca geothermal field for I-S mixed-layer mineral characterization, using XRD, SEM, and HRTEM. The samples were collected from 262 to 408 m depth range (corresponding to an 80–180 °C T range), at which depths the smectite to illite transition was detected by XRD study (Vázquez et al., 2014). The main characteristics of the selected samples are summarized in Table 1. The sample labels correspond to their depth.

3.1. X-ray diffraction

The samples were crushed with a laboratory jaw-crusher. The <2 μm fraction was separated by centrifugation, and then smeared onto glass slides. The XRD data were obtained with a Bruker D8 Advanced diffractometer with Cu-Kα radiation and Bragg–Brentano geometry at the University of Chile (Chile). Clay minerals in this fraction were identified according to the position of the basal reflections on XRD patterns of air-dried, ethylene-glycolated (EG) and heated (300 °C for 2 h). I-S mixed-layer clay minerals were identified and the respective proportions of illite components determined according to Moore and Reynolds (1997) criteria. Heat treatments were useful in identifying

Table 1
Drill hole sampling carried out in Pte-1 well along with clay mineralogy (XRD) and dioctahedral clays identified by TEM.

Sample (drilling depth)	T (°C)	Lithology	XRD data							TEM data
			Sme	Be	I-S		Chl	LC-Corr	Chl-Vrm	
					R	% Ilt				
262	80	Porphyritic andesite with amygdalus (+yr)	X	X	-	-				Sme (+I1)
281	85	Argillized tuff (+hem + pyr + cal)			R0	30	X	X		Sme (+I1 + I > 1)
282	85	Argillized tuff (+hem + pyr + cal)			R0	10	X		X	−I1 + Ilt (+Sme + I > 1)
					R1	40				− I1 + Sme
						60				
325	125	Argillized tuff (+silica + pyr + cal)			R1	60	X	X	X	I1 (+I > 1 + Ilt)
328	130	Argillized tuff (+silica + pyr + cal)			R1	70	X	X	X	–
408	175	Silicified tuff (+cal)			R3	90	X	X	X	Ilt (+I > 1)

Mineral abbreviations as suggested by Whitney and Evans (2010): Sme: Smectite, Be: berthierine I-S: Illite-Smectite mixed layers, Ilt: Illite, Chl: Chlorite, LC-Corr: Low-charge Corrensite, Chl-Vrm: Chlorite-Vermiculite mixed layers, Pyr: Pyrite, Hem: Hematite, Cal: Calcite. Nomenclature for interstratifications in the TEM study as proposed by Bauluz et al. (2000).

vermiculite layers in the chlorite mixed-layer phases. Overlapping peaks of mixed-layer clay minerals were separated by decomposition procedures using MacDiff 4.2.5 (Petschick, 2000).

3.2. Electron microscopy

Polished sections of the six samples were analysed by field emission SEM (FESEM) at the University of Zaragoza (Spain) using backscattered electron (BSE) and semi-quantitative analysis by energy-dispersive X-ray (EDS) to obtain textural and chemical information. The accelerating voltage was 4 to 15 kV with a beam current of 1–2 nÅ and a counting time of 50 s for analysis. Samples were coated with carbon for BSE imaging and EDS analysis.

Based on the XRD and SEM results, five samples were selected for the HRTEM study. TEM, in combination with XRD, enhances the characterization of clays and mixed-layer I-S minerals. TEM techniques provide information on the nanotexture, crystal structure, and quantitative chemical data from precise areas. An essential problem in the TEM investigation of mixed-layer I-S minerals is the collapse of expandable interlayers under high vacuum, which makes the distinction between smectite and illite layers in I-S very difficult, if not impossible. Improvements in imaging and sample preparation techniques have addressed this problem by ensuring the permanent expansion of smectite interlayers using LR white resin (Kim et al., 1995; Bauluz et al., 2000, 2002; Yan et al., 2001; Tillick et al., 2001) and using the imaging conditions indicated by Guthrie and Veblen (1989a, 1989b, 1990). Samples were treated with LR white resin following the procedure of Kim et al. (1995) in order to prevent the collapse of smectite-like interlayers in the vacuums of the ion mill and TEM, as well as to facilitate the differentiation of illite and smectite interlayers in TEM images. Great care was taken to prevent direct contact with water during sample preparation in order to avoid smectite expansion and resultant sample damage. Sticky wax-backed thin sections were prepared and first examined by optical microscopy. Typical areas were removed for TEM observation via attached Cu washers, thinned in an ion mill, and carbon coated. In order to identify areas of interest for the TEM study, the ion-milled samples were studied by FESEM. HRTEM observations were performed using a Jeol-2000 FXII equipped with an Oxford instrument detector (EDS) at the University of Zaragoza (Spain). The TEM was operated at 200 kV and a beam current of 20 mA. In order to obtain the imaging conditions described by Guthrie and Veblen (1989a, 1989b, 1990), through-focus series of images were obtained from 1000-Å underfocus (approximate Scherzer defocus) to 1000-Å overfocus, in part to obtain optimal contrast in I-S ordering (overfocus). However, because the initial focus was controlled manually by minimizing contrast, small deviations from exact underfocus or overfocus numbers were inevitable. Individual particles of clay minerals were chemically analysed in a Philips CM-20 scanning TEM (STEM) at the University of Granada (Spain), working at 200 kV with a point-to-point resolution of 2.7 Å in the TEM mode. Chemical compositions were obtained from powdered portions, dispersed onto C-coated Au grids. We used the STEM mode with a 50 Å beam diameter with an EDS microanalysis system.

3.3. Nomenclature for interstratifications

Ordering in interstratified I-S is ordinarily characterized by its Reichweite value, on the basis of X-ray diffraction data. Such measurements of I-S ordering represent long-range ordering averaged over all the layers that scatter X-radiation. However, short-range ordering of interlayers within I-S packets can be identified in TEM images. The Reichweite nomenclature is therefore inappropriate for specific layer sequences as observed by TEM. For the purpose of this study, we employ the nomenclature proposed by Bauluz et al. (2000), using the notation I*n*, where *n* is the number of illite-like layers associated with a given smectite-like layer (i.e., IS-IS- layers are denoted as I1 units, ISI-ISI- as I2 units). This nomenclature is analogous to the Reichweite nomenclature, but applied only to specific layers. An ideal (rectorite) sample for which $R = 1$, having 50% illite-like layers, is identical to a sequence of I1 units, but a sequence for which $R = 1$ and I% >50% would consist dominantly of I1 units, but would also have I2, I3… units ($n > 1$).

4. Results

4.1. X-ray diffraction

Clay minerals identified in the <2 μm fraction are shown in Table 1. Smectite, berthierine, chlorite and mixed-layer minerals (such as I-S, corrensite, and chlorite-vermiculite mixed layers) are the clay phases identified in the samples. I-S mixed layers have been identified by comparing the air-dried and ethylene glycol-treated specimens (Fig. 2). The illite proportion in I-S was determined by the position of the reflections near 9° to 11° 2θ (Fig. 3A) and near 16° to 17° 2θ (Fig. 3B) and the R parameter by the position of the reflection from 5° to 8.5° 2θ for EG-solvated preparations (Fig. 2). The coexistence of R0 and R1 I-S minerals has been observed in the XRD data of sample 282 (Fig. 2). Peak decomposition using MacDiff (Petschick, 2000) suggests that the 001/002(EG) peak for I-S at 282 is comprised of overlapping components at ~9.34, 8.99, and 8.53 Å (Fig. 3A); the 002/003 (EG) peak can be decomposed into overlapping components at 5.59, 5.48, and 5.36 Å (Fig. 3B). While peak decomposition likely does not produce a unique solution, it is consistent with a mixture of R0 I-S 10% I, R0 I-S 40% I, and R1 I-S 60% I.

Chlorite-like phases have been detected in the illitization sequence. Corrensite was identified by the presence of characteristic reflections in EG treatments such as 31 Å, 15.5 Å, and 7.8 Å, which correspond to (001) (002) and (004) reflections. Moreover, heat treatment at 300 °C

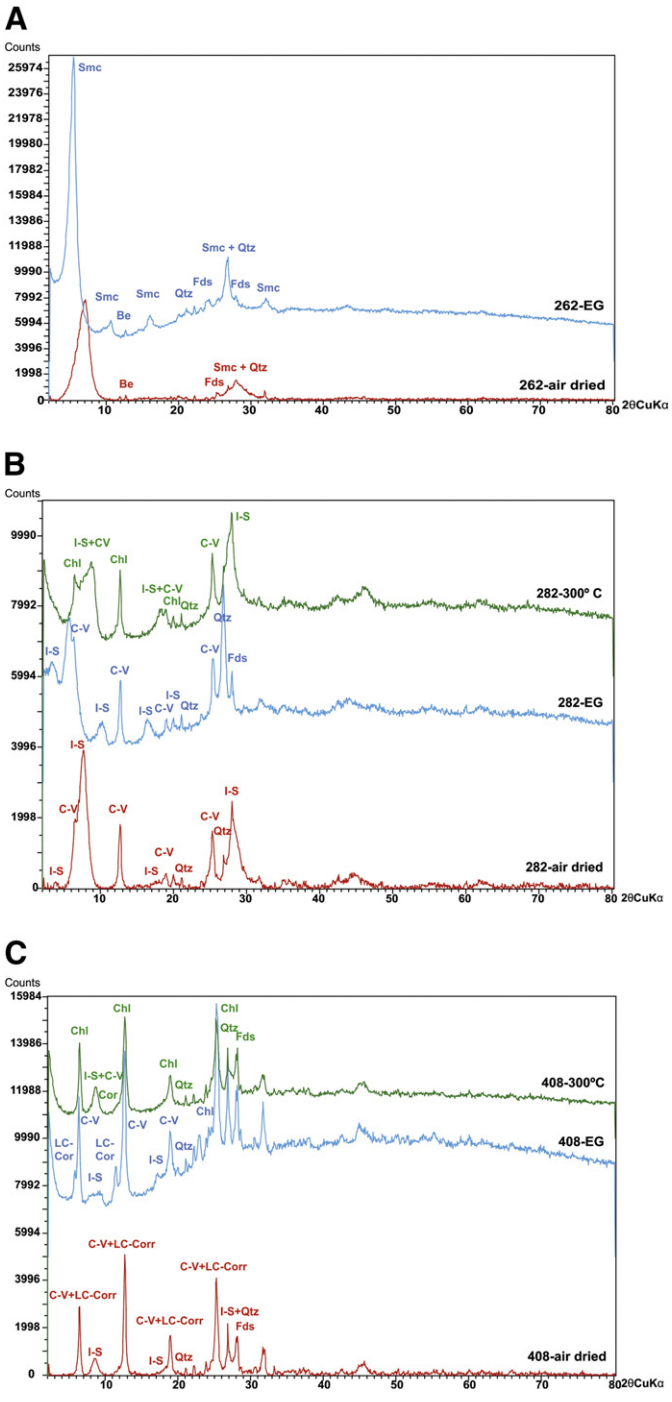

Fig. 2. XRD patterns corresponding to <2 μm oriented fractions of samples 262, 282, and 408.

for 2 h shows one plateau with spacing ranging from 7 to 8 Å (Fig. 2), which is interpreted as a convolution of 002 (~7 Å) of chlorite and 003 (~8 Å) of collapsed corrensite. Heat treatments also reveal the presence of a chlorite-vermiculite mixed layer in some samples. The peaks corresponding to such mixed-layers do not change with the EG treatments, but collapse after heating to 300 °C (Moore and Reynolds, 1997). The presence of vermiculite layers generates significant changes in the intensity and basal spacing of chlorite. Therefore, the 001 of chlorite shows a spacing of 14.3 Å in air-dried samples, but the characteristic peak of chlorite is found at 14.01 Å in heated samples.

The distribution of phyllosilicates along the illitization sequence shows depth-based zoning. Dioctahedral smectite together with berthierine are the main clay minerals in the shallowest sample. Below, I-S mixed-layer minerals are the primary dioctahedral phase and smectite is absent. The illite layers and ordering type of I-S minerals increase with depth, from R0 I-S (30% I) at 281, the coexistence of two R0 I-S (10 and 40% I) and R1 I-S (60% I) at 282, R1 I-S (60% I) at 325, and R3 I-S (90% I) at 408. Chlorite appears together with I-S minerals, but low-charge corrensite and chlorite-vermiculite along the sequence is discontinuous (Table 1).

4.2. Scanning electron microscopy

Representative BSE images of the six samples are presented in Fig. 4. Unaltered tuffs are composed of phenocrysts of Ca-rich plagioclase, rounded fragments of volcanic glass, and a groundmass of Ca-rich plagioclase and glass.

Sample 262 has a typical texture formed of volcanic glasses, plagioclase phenocrysts, and matrix (Fig. 4A). Volcanic glass is completely altered to smectite whereas plagioclase phenocryst alteration is scarce. The clasts are imbedded in a matrix of minute plagioclase microliths and clays with smectite-like composition that probably replaced the original vitreous matrix (Fig. 4B). High-magnification images of the matrix show that smectite packets exhibit a curved (sometimes circular or semi-circular) lens-shaped morphology, with no preferred orientation (Fig. 4C). Curved packets of smectite with a discontinuous circular shape commonly surround cores. The cores look empty, which probably indicates that the dissolution of the amorphous material of the matrix was complete.

As illustrated in Fig. 4D–I, samples 281, 282, 325, 328, and 408 comprise plagioclase phenocrysts, Ti-magnetite and plagioclase as microliths, pseudomorphs of vitreous fragments with rounded morphologies replaced by dioctahedral clays (I-S and illite), and a clay-rich matrix, that previously consisted on glass, also formed of mixed-layer I-S and illites. Plagioclase phenocrystals in all the analysed samples show scarce evidences of alteration. In the most altered samples (328 and 408), discrete silica phase (quartz) crystals and partially albitized plagioclases have also been observed. The dioctahedral clays of the matrix of these rocks have a filamentous texture indicating an in situ crystallization.and are associated to Fe-rich chlorites, scarce apatite, and primary relict Fe-Ti oxides.

The SEM study of the analysed samples shows that the vitreous phases have been replaced by Sm, I/S or illite. In contrast, plagioclase phenocrysts are only scarcely altered. Texture of the dioctahedral clays reflect they crystallized directly from fluids.

4.2.1. Chemical composition of dioctahedral clays

Based on the EDS analyses, the clays in sample 262 are dioctahedral smectites and can be classified as montmorillonite (Fig. 5, Supplementary data). They have $Al^{VI} > Fe + Mg$, low tetrahedral substitutions ($Al^{IV} < 0.05$ apfu), an interlayer charge of ~0.40 apfu, and interlayer positions occupied by Ca > K > Na. There are no significant compositional differences among the smectites that replace plagioclases, glass clasts, or the vitreous matrix. EDS analyses of clays from samples 281, 282, 325, 328, and 408 indicate that they are also dioctahedral clays. In all cases, they are Al-rich clays with $Al^{VI} > Fe + Mg$, and the interlayer site is composed of Ca and K with very low Na contents. From the EDS data (supplementary data) and XRD results, we infer that these clays are different types of mixed-layer I-S and illitic phases.

Combining the XRD data and SEM/EDS analyses, we can conclude that the composition of clays from sample 281 correspond to R0 I-S. In sample 282, two types of compositions have been distinguished, those forming a matrix with a similar composition to that of clays from 281 that would correspond to R0 I-S and the clays that pseudomorphize vitreous fragments corresponding to R1 I-S. The compositions of R1 I-S have lower Si contents and larger interlayer charges in comparison to R0 I-S (Fig. 5). According to XRD, I-S mixed layers of 325 and 328 correspond to R1 I-S, and their compositions are similar to the R1 I-S from

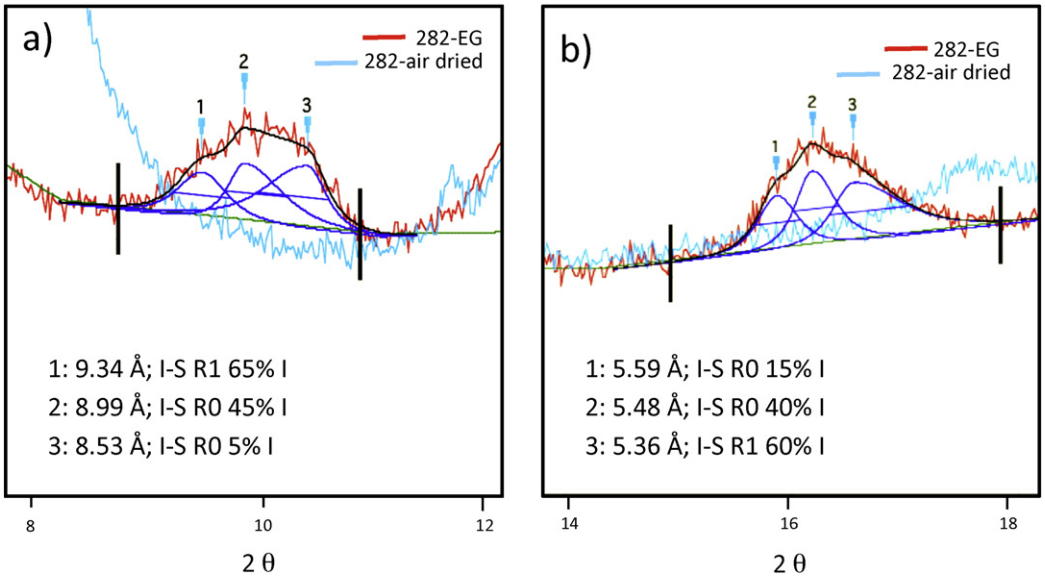

Fig. 3. Decomposed XRD patterns of sample 282.

sample 282, and the mixed-layer I-S from sample 408 corresponds to R3 I-S and/or illites.

Fig. 5a shows that there is a decrease in the Si contents and an increase in the interlayer charge and in the K contents with the alteration grade, indicating progressive illitization from sample 262 to 408 (Supplementary data). The illitization produces, therefore, an increase in the substitution of Si by Al, but with no significant changes in the Al^{VI}/Fe + Mg ratio.

The compositional variations in these dioctahedral clays are characteristic of metastable phases formed under low-temperature conditions.

4.2.2. Chemical composition of plagioclase phenocrysts

EDS analyses of plagioclase indicate that they have intermediate compositions between anorthite and albite end-members. Fig. 5 shows the variations in the Ca vs Si content of the analyses. Most of them plot forming a group that ranges from 2.47–2.72 apfu of Si and 0.29–0.56 apfu of Ca, and the average composition of the group corresponds to Ab_{52} An_{44} Or_{3}. This composition is consistent with the interval composition of primary plagioclase in equilibrium with basaltic andesite to andesitic melts. In contrast, Si-rich and Ca-poor analyses, plotting outside the primary group, correspond to totally or partially albitized plagioclases from the most altered samples and probably produced by geothermal alteration.

4.3. Transmission electron microscopy

TEM observations of the five analysed samples are described below in order of increasing degree of illitization. A summary of the dioctahedral clays and I-S depicted in the TEM images is shown in Table 1.

4.3.1. Sample 262 (smectite)

As shown in Fig. 6A, this sample contains smectite with the typical texture when it is formed by the replacement of volcanic glass. Smectite exhibits straight, curved, and sometimes circular or semi-circular packets, with no preferred orientation. The smectite is characterized by discontinuous, wavy fringes with spacings from 12 Å to 14 Å (most commonly 12–12.5 Å) and even the spacing varies through the layers (Fig. 6B). The d values depend on the degree of dehydration and layer collapse caused by interaction with the electron beam or the TEM or ion-mill vacuums. There are abundant layer terminations and the boundaries between packets are diffuse and appear to grade into the matrix (Fig. 6B-C). No glass has been imaged, indicating it was probably completely replaced by smectite.

SAED patterns show diffuse low-order 001 reflections, and non-00 l reflections are ill-defined, non-periodic, and diffuse parallel to c* (inset in Fig. 6B). They have characteristics of poorly crystalline smectite, perhaps mixed with amorphous material.

Occasionally, the alternating dark and light contrast typical of mixed-layer I-S (Guthrie and Veblen, 1989a, 1989b, 1990; Veblen et al., 1990) has been noted. Moreover, these fringes have spacings (21- to 22-Å periodicity) characteristic of the sum of illite- and smectite-like layer spacings in R1 I-S (Kim et al., 1995; Dong et al., 1997) (Fig. 6C). We use the term I1 for such individual units, as described above.

4.3.2. Sample 281 (I-S R0 35)

TEM images of the matrix of this sample show thin curved packets of smectite with thicknesses ranging between approximately 5 and 20 nm (Fig. 7A). The morphologies imply that it precipitated directly from interstitial fluids. Smectite has similar characteristics as in sample 262, showing discontinuous, wavy fringes with spacings from 12 Å to 14 Å (Fig. 7B). SAED patterns have diffuse low-order 001 reflections, and non-00 l reflections are ill-defined, non-periodic, and diffuse parallel to c* (inset in Fig. 7B). Additionally, there are some layers comprising I1 (21- to 22-Å periodicity) and I2 (31- to 32-Å periodicity) units (Fig. 7C and D).

4.3.3. Sample 282 (I-S R0 10 + I-S R0 40 + I-S R1 60)

As mentioned in the SEM results, EDS analyses have shown the coexistence of two different types of mixed-layer I-S in this sample: the matrix is formed by I-S R0 and the glassy fragments are replaced by R1 I-S. Fig. 8A shows both types of clays and their textural relations. Fig. 8B–C display TEM textural images of the areas indicated in the BSE image shown in Fig. 8A.

I-S phases replacing glassy fragments show a fan-like texture (Fig. 8B), whereas those of the matrix have a filamentous texture similar to the matrix in sample 281 (Fig. 8C). Both texture suggest a direct crystallization from hydrothermal fluids. As a consequence of texture differences, the clay fabric of the matrix is more porous than in fragments. HRTEM images show the coexistence of smectite (Fig. 8D) and layers comprising I1 (21- to 22-Å periodicity) in the matrix. The fragments consist of I1 units (Fig. 8E) and illite packets (Fig. 8F) with only occasional smectite and I-S I> 1. As in lower-T samples, the

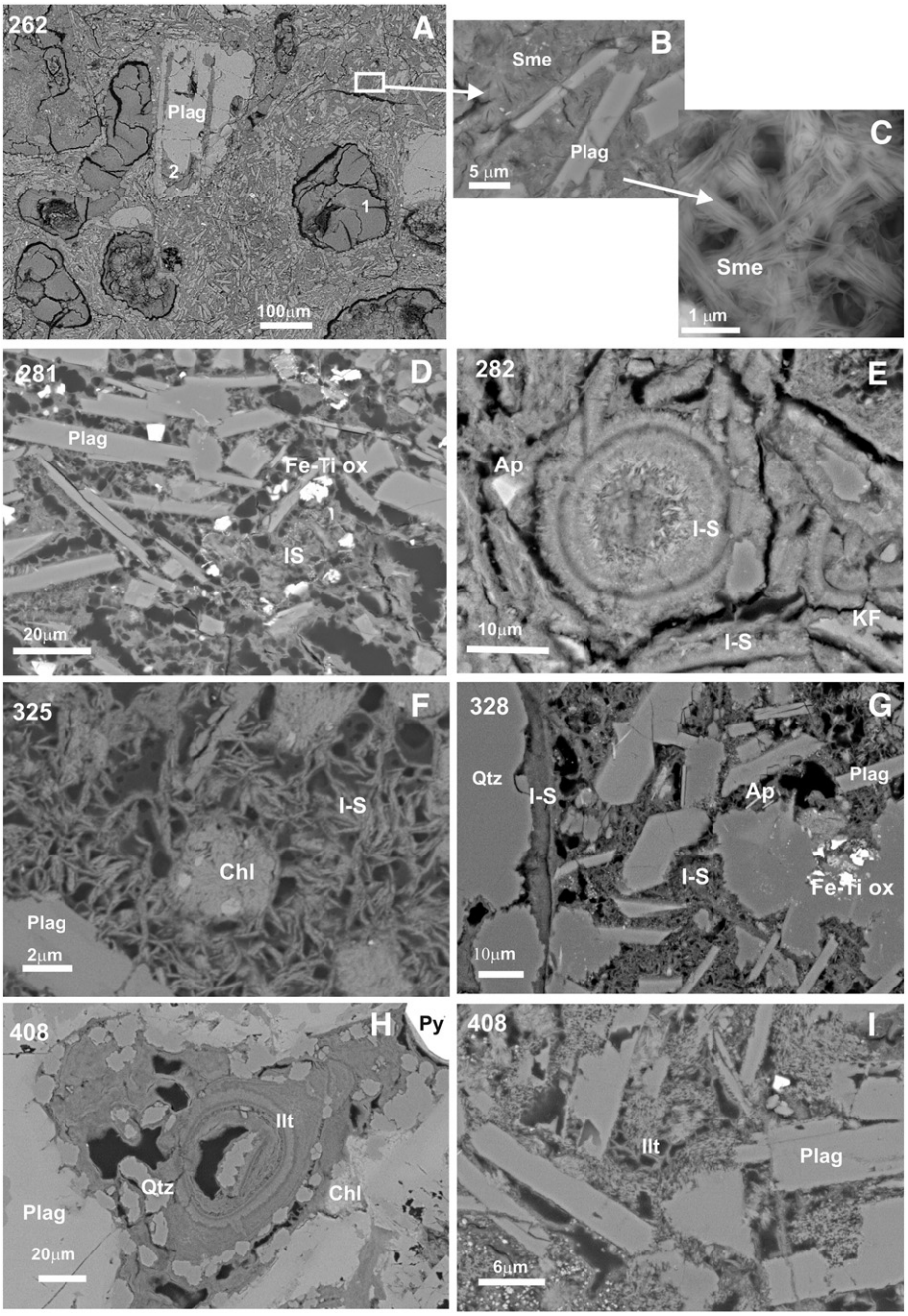

Fig. 4. SEM/BSE images of samples 262 (A–C), 281 (D), 282 (E), 325 (F), 328 (G), and 408 (H–I).

boundaries of the smectite and I-S packets are diffuse, with abundant layer terminations. In contrast, illite crystallites have straight lattice fringes with constant 10-Å spacings. They are 10–15-nm thick with relatively well-defined boundaries (Fig. 8F). SAED patterns of smectite and I1 units are similar to those of smectite of lower-T samples with diffuse low-order 001 reflections.

4.3.4. Sample 325 (I-S R1 60)

Clays from sample 325 have the filamentous, porous texture described in previous samples (Fig. 9A). HRTEM images indicate that they consist of areas rich in I1 units with accessory illite packets and I> 1 (Fig. 9B-C). SAED patterns (insert in Fig. 9B and C) are consistent with those of typical 1Md polytypism and are relatively better defined than those of upper-level (lower T) samples.

4.3.5. Sample 408 (I-S R3 90)

Textural images indicate the hydrothermal dioctahedral clays are randomly oriented (Fig. 10A), as shown in previous samples. HRTEM images show that they are formed of nearly straight lattice fringes with constant 10-Å spacings (Fig. 10B). They are 5–15 nm thick, with relatively well-defined boundaries. Occasionally, I3 units have been observed. SAED patterns of illite are characteristic of 1Md polytypism. Fig. 10B shows some continuity among illite and plagioclase layers, suggesting topotactic growth.

4.3.6. AEM analyses of dioctahedral clays

The chemical composition of the clays corresponds to dioctahedral phases (Supplementary data). In some analyses, the octahedral charge could be considered slightly higher than normal. This may be because

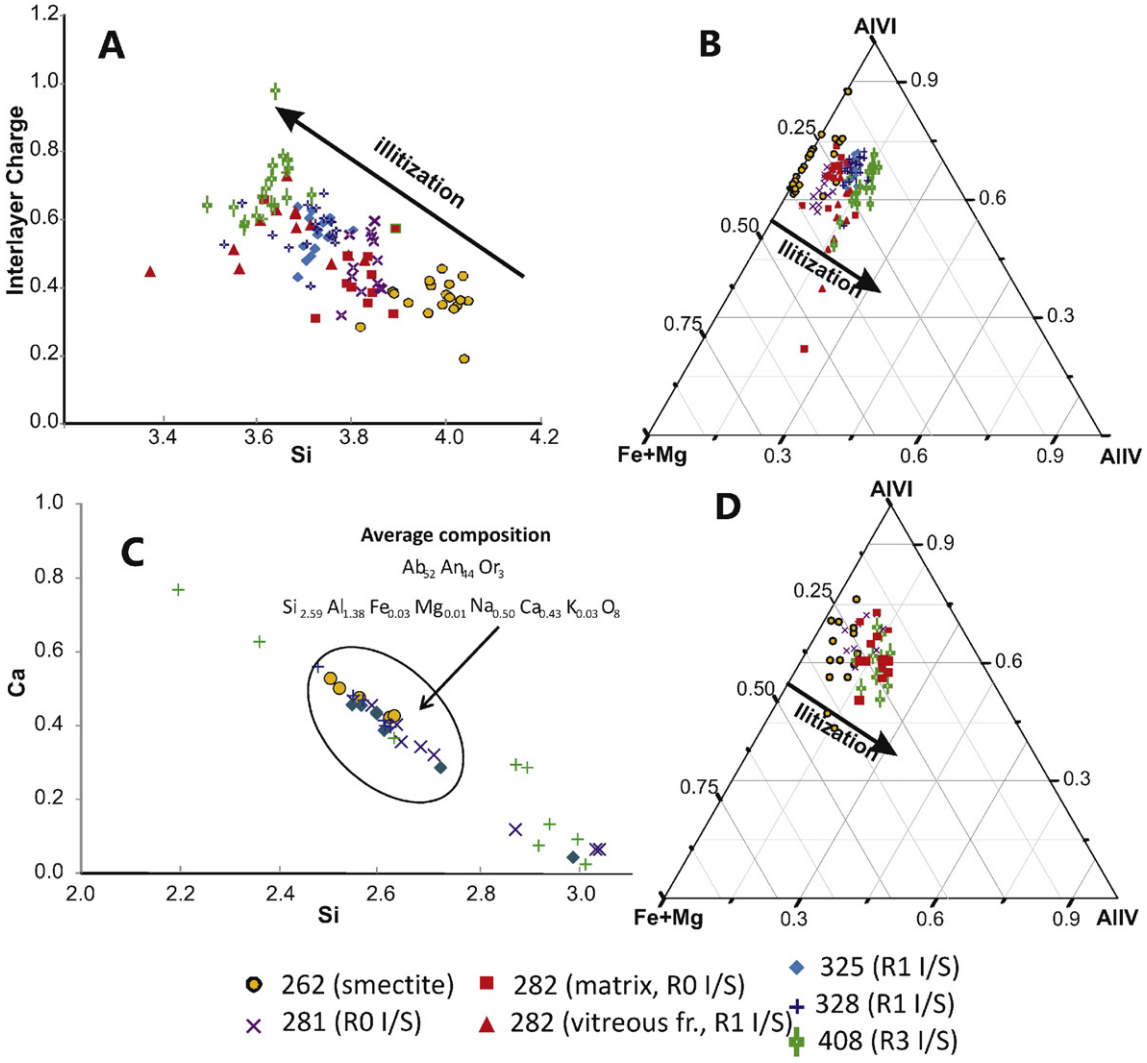

Fig. 5. SEM-EDS analyses of dioctahedral clays plotted on (A) the Si vs. interlayer charge graph, (B) the Fe + Mg − Al^{VI} − Al^{IV} graph, and (C) plagioclases: Si vs Ca. TEM-AEM compositions of dioctahedral clays plotted on (D) the Fe + Mg − Al^{V} − Al^{IV} graph.

all the Mg has been assigned to the octahedral layer, even though this cation can also be present in part in the interlayer position. In the absence of a valid distribution criterion, we have not attempted to distribute the Mg between the two structural positions.

The two analytical techniques (SEM/EDS and TEM/AEM) have defined similar trends of chemical composition evolution with depth (Fig. 5). AEM analyses reveal smectite from sample 262 has slightly lower Si contents (3.96–3.63 apfu) than the corresponding analyses performed with EDS. AEM analyses also indicate that smectite has a montmorillonite-nontronite composition with a significant beidellite component. In general, for all the samples, the AEM chemical analyses are clearly more heterogeneous at the sample level than those in EDS (Fig. 5). AEM data correspond to chemical analyses of individual particles of clay minerals instead of areas analysed by EDS in grain minerals, in which, presumably, average compositions of the various particles included in the analysed area are obtained, thereby reducing the overall range of compositions.

Samples 281 to 408 show a trend of decreasing Si contents and increasing interlayer charges, indicating a progressive illitization (Fig. 5).

5. Discussion

The Tinguiririca geothermal field, as analysed from the Pte-1 drill core samples, evidences a typical alteration pattern with argillic alteration in the upper part evolving to propylitic alteration in depth. Clay minerals also show an evolution pattern typical of these high-gradient geothermal alteration processes, with smectite being the most stable phase in upper levels and evolving to illite and chlorite in depth. Moreover, the smectite-to-illite sequence has been observed in the samples collected from 262 to 408 m depth range and corresponding to an 80–180 °C T range, revealing its progress under metastable and kinetically controlled conditions.

5.1. Comparison between XRD and electron microscopy data

The illitization sequence detected by XRD is apparently continuous from smectite to R3 I-S through R0 and R1, with a progressive increase in illite layers (Table 1). Hence, it reproduces the commonly described sequence in the traditional literature for both hydrothermal and diagenetic environments.

The TEM data show a similar illitization trend (Table 1). However, the high-resolution images reveal that the analysed clays are more heterogeneous than the XRD patterns reflect, illustrating the coexistence of different types of dioctahedral clays. The TEM images also indicate that the most abundant dioctahedral clays are smectite, I1 I-S, and illite, so the XRD patterns are probably the result of the mixture of these phases plus accessory I-S mixed layers having higher ordering. Therefore, the actual sequence is not as continuous as XRD seems to indicate. On the

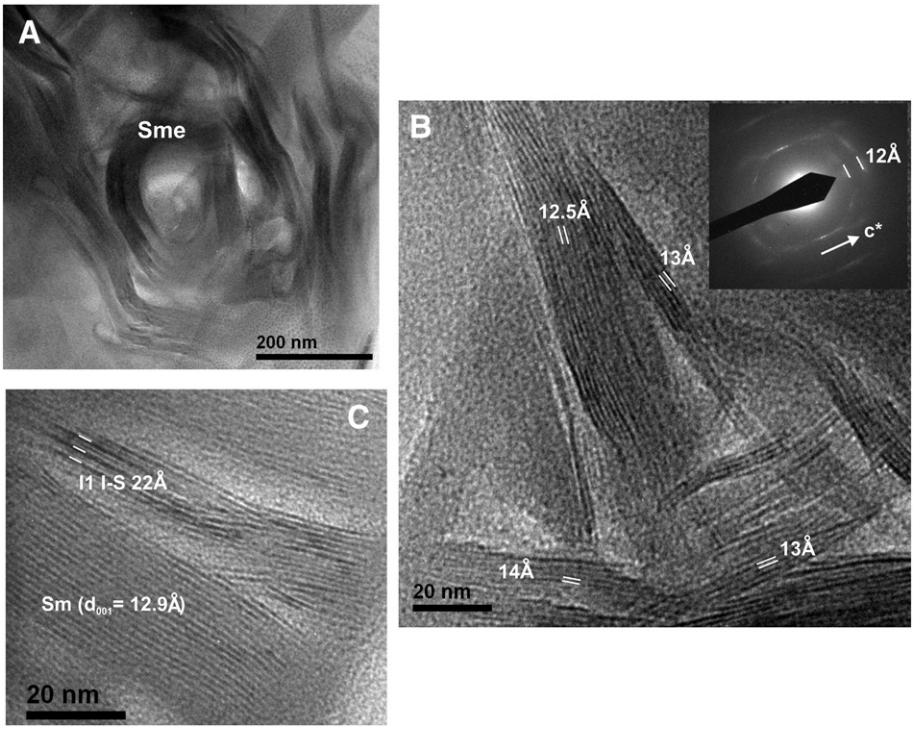

Fig. 6. TEM images of sample 262. Low magnification (A) and lattice-fringe images and SAED patterns (B-C).

other hand, the combination of SEM and TEM reveals that, in sample 282, clays formed from the glassy matrix are smectite and I1 I-S, and those formed from vitreous clasts are I1 I-S plus illite.

Even though TEM images do not show abundant I0 or I3 I-S, their occurrence in minor proportions in the analysed samples cannot be discarded. A smectite layer impregnated with LR white resin collapses to 11–13 Å and it can therefore be complicated to distinguish illite layers between predominant smectite. In the case of R3, differences in identification of this I-S between XRD and TEM may be due to the fact that the LR white resin cannot diffuse into interlayers, but only maintains the

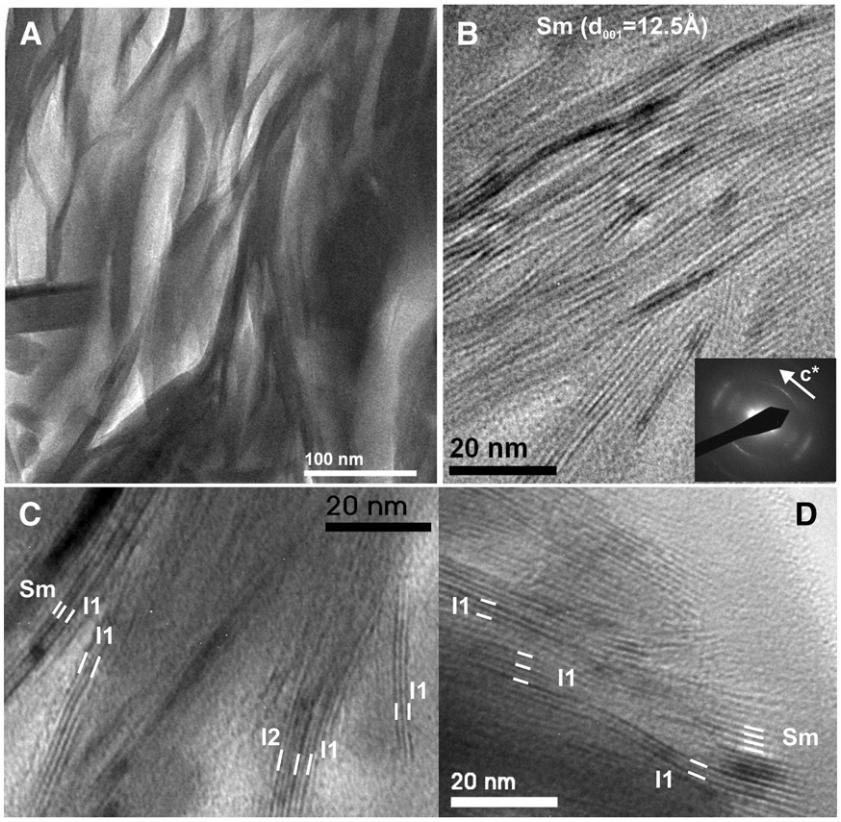

Fig. 7. TEM images of sample 281. Low magnification of the matrix (A) and lattice-fringe images and SAED patterns (B–C–D) showing smectite and I-S units.

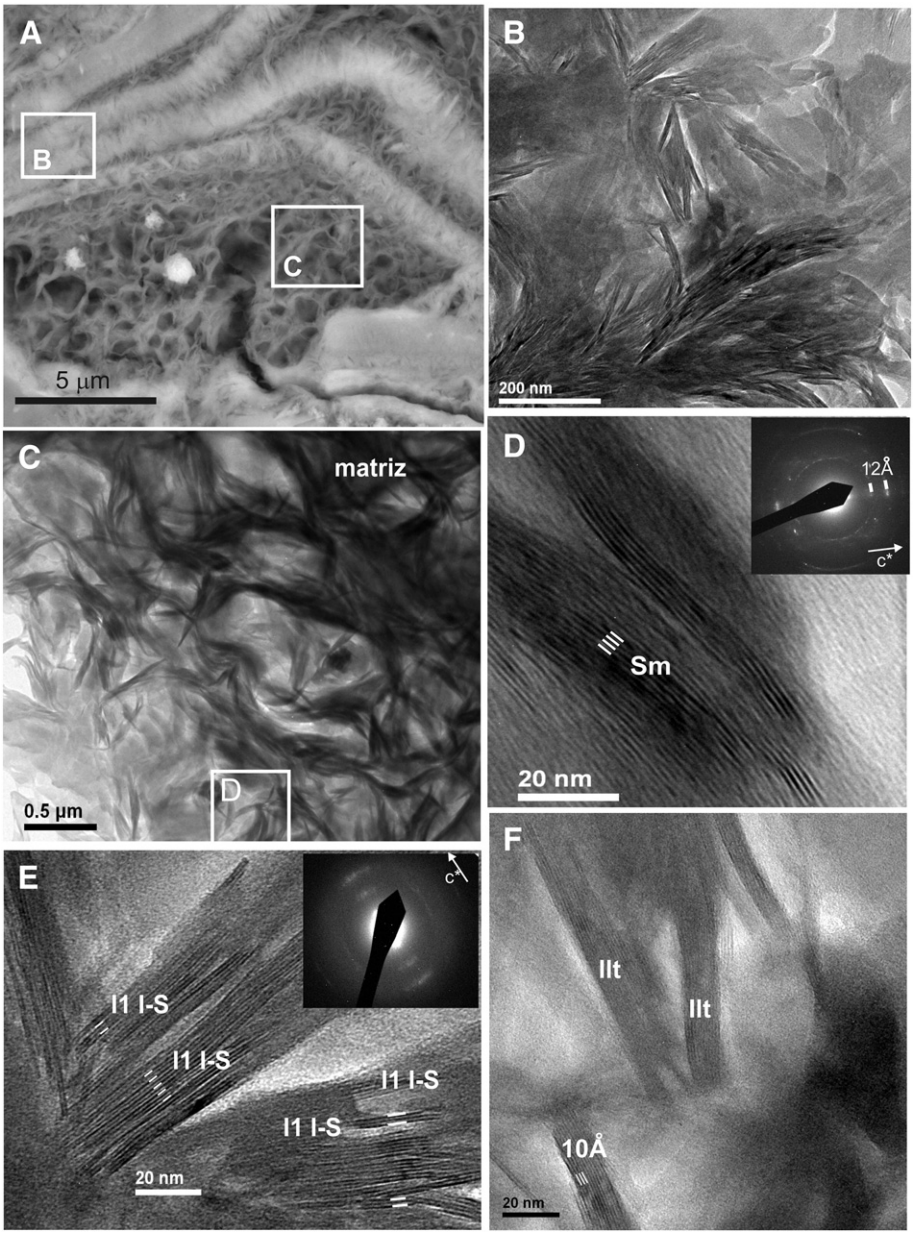

Fig. 8. Electron microscopy images of sample 282. SEM/BSE image (A) showing the texture of clays that have replaced vitreous fragments (rectangle B) and the glassy matrix (rectangle C). Low-magnification TEM images showing the texture of clays that have replaced vitreous fragments (B) and the glassy matrix (C). Lattice-fringe image corresponding to clays that form the matrix (D) and vitreous fragments (E, F).

dimensions of the untreated sample, in contrast to the action of ethylene glycol, as Bauluz et al. (2002) suggested. Additionally, we should also consider that Guthrie and Veblen (1989a, 1989b, 1990) pointed out it is sometimes not possible to obtain images that allow the differentiation of smectite and illite layers, thus biasing the TEM results.

However, we are not aware of any TEM study describing predominant I0 or I3 ordering despite the large numbers of such studies of I-S sequences; for instance, TEM observations similar to those of this study were reported by Dong et al. (1997) and Bauluz et al. (2002). In agreement with the present case, their results, which showed the presence of smectite, illite, and ($R = 1$) I-S but not I0 I-S or I3 I-S, were inconsistent with the XRD data reported for the same samples.

5.2. Changes in chemical composition of dioctahedral clays with illitization

The chemical composition of the analysed dioctahedral clays indicates that they have higher Al contents in the octahedral sheet in comparison to Mg and Fe. The most significant compositional trend with illitization is the increase in Al in tetrahedral positions, which is compensated by the increase in the interlayer charge. The interlayer sites are mainly occupied by K and Ca, with an increasing K/Ca ratio with illitization. Although analyses from different samples overlap each other, there are clear differences between them in agreement with the composition of the respective dominant clays (e.g. smectite, R1 I-S, or illite), even in sample 282 in which smectite (or R0 I-S) coexists with R1 I-S in different textural sites. The overlapping analyses may be a consequence of chemical heterogeneity of the phases and the coexistence of different kinds of phases at the sample level, but also of the technique used for the analyses. The SEM electron beam has a spot size larger than the clay particles, and each analysis includes a group of particles. Therefore, it is equivalent to a type of physical averaging of the various compositions found in the sample. AEM analysis, performed in the TEM, tries to take advantage of its higher spatial resolution to analyse individual particles and it has shown more clearly

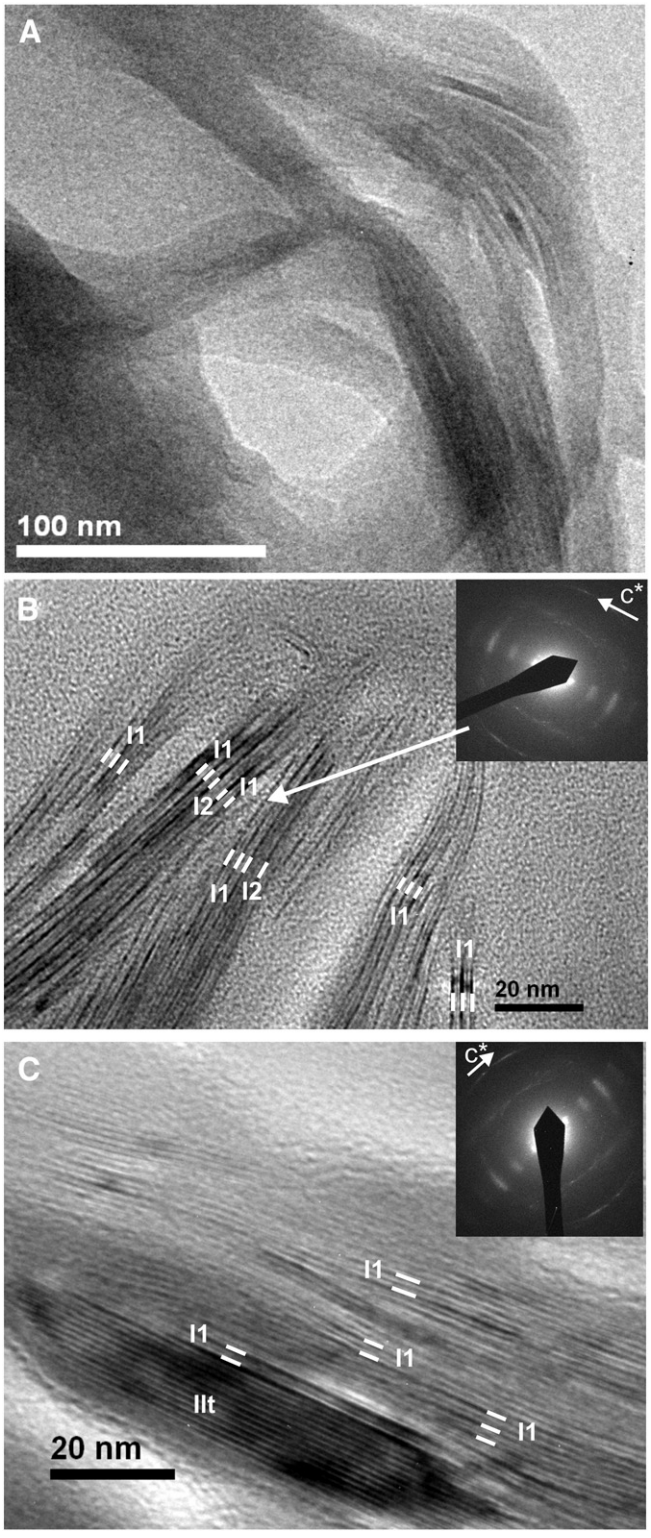

Fig. 9. TEM images of sample 325. Low magnification (A), and lattice-fringe images and SAED patterns (B—C).

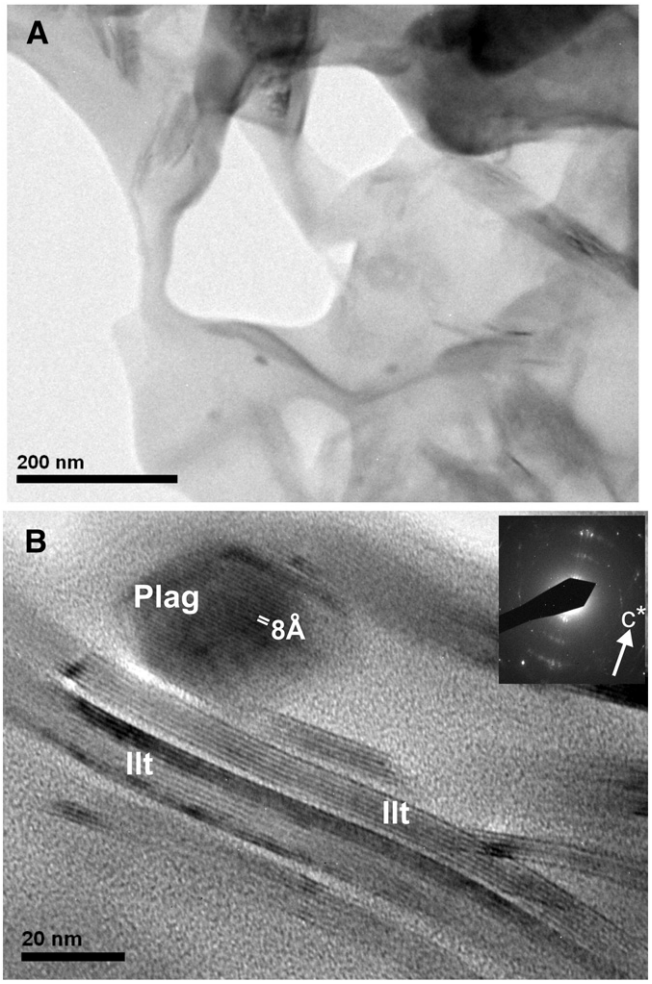

Fig. 10. TEM images of sample 408. Low-magnification (A) and lattice-fringe image and SAED pattern (B).

their heterogeneous nature. The differences revealed by the SEM analyses are a consequence of the various possible combinations of the composition range detected by AEM. Although the variations shown by AEM are higher than those of SEM, the two techniques show similar trends and ranges, with the small differences motivated partly by methodological bias and partly by the possible inclusion of minor quantities of other mineral phases depending on the size of the analysed area.

5.3. Crystallization mechanism

One of the main topics in illitization sequences in active geothermal systems concerns the precise mechanism that allows this clay mineral evolution under a high gradient and under different fluid/rock ratios. A recent paper from Beaufort et al. (2015) illustrates the different crystallization mechanism in the chloritization processes through mixed-layer mineral series in low-temperature geological systems. According these authors, smectite to chlorite transition differs in diagenetic from hydrothermal systems. The main conclusions of these authors about the different crystallization mechanism are in relation with drastically different heating rates, heat flow conditions and tectonism between basins under passive tectonic regime against geothermal systems in active margins. In the Tinguiririca geothermal system, it is clear from our results that illitization is mostly T-controlled. However, as Inoue et al. (2004) showed, illitization is also a kinetically controlled process that occurs in active geothermal systems within a relatively short time.

The BSE images of our samples show that the clasts of glasses and the matrix, previously formed of glass, consist of dioctahedral clays. This means that vitreous components have been completely replaced by the clays (e.g. smectite, I-S mixed layers, and illite) after fluid-rock interactions. In contrast, crystalline components of the rocks show only minor evidence of re-emplacement by clays (Fig. 4). The textures observed in SEM provide evidence for clay crystallization from a fluid following the dissolution of precursor glassy metastable phases. Therefore,

this study shows that the formation of I-S and illite phases did not require precursor smectite; in all analysed samples, they form from the dissolution of glass components and crystallization from fluids. Indeed, transitions from smectite to I/S or Illite layers have been not observed by HRTEM. The crystallization of smectite, I/S or illite in this samples mainly depends on the T of the hydrothermal fluid as other authors reported in similar environments (Bauluz et al., 2002; Inoue et al., 2004, 2005; Murakami et al., 2005, among others). The nature of the alteration and the type of neoformed clays imply that the hydrothermal alteration at the Tinguiririca geothermal field took place at low T increasing with depth, as previous data show (Vázquez et al., 2014).

As mentioned above, the TEM data reflect that the alteration produces the crystallization of a discontinuous illitization sequence with the formation of smectite, R1 I-S, and illite as the most abundant phases, indicating that they are relatively more stable than random mixed-layer I-S. However, certain authors (Lippmann, 1982; Jiang et al., 1990; Essene and Peacor, 1995) consider illite, I-S, and smectite to be metastable phases in all occurrences in comparison to assemblages containing muscovite, as shown by pelitic rocks approaching equilibrium at greenschist-facies conditions. As we show in this study, these minerals are chemically and texturally heterogeneous with a high degree of disorder and their crystallization follows the Ostwald step rule (Morse and Casey, 1988; Inoue et al., 2004). The crystallized phase at each microsite in the sample depends on local factors such as the composition of the precursor and differences in T and/or fluid composition.

Although several mechanisms have been proposed for illitization, two of them represent the extremes: layer-by-layer replacement and bulk dissolution-crystallization. We have not observed any layer-to-layer transition that would support layer-by-layer replacement. The hydrothermal fluid probably partially dissolves the original rock and the clays simultaneously crystallize from the fluid. The fluid characteristics (T and composition) favour the dissolution of the vitreous material, which is more unstable and reactive than the crystalline components.

The illitization and the crystal chemistry of mixed-layer I-S depends on the T, fluid composition, time, the fluid/rock ratio during the formation of I-S minerals, and the chemical composition of the precursor materials (Altaner and Ylagan, 1997). All these factors must be considered at an extremely local scale due to the lack of equilibrium at the sample level. Therefore, there is a predominant phase for each sample, or at least for each textural position (e.g. sample 282), but other phases can also be present depending on the aforementioned local factors.

In the study case, The Tinguiririca geothermal field developed in Holocene to Pliocene volcanic rocks related to K-rich calc-alkaline lavas. A strong kinetic control seems to be involved in the illitization sequence in this active geothermal system. Taken into account the age of the altered volcanic rocks, the timing needed to achieve the illitization mineral reaction must be in the order of 1×10^3 to 1×10^4 years, far away from the typical timing observed in sedimentary basins (see Beaufort et al., 2015). Over these high heating rate conditions, mineral reactions must be mostly out of equilibrium and there are consequently two critical factors controlling the illitization process: T availability and K availability (which favours the crystallization of clays progressively richer in K). As previously mentioned, K_2O values in this type of calc-alkaline andesites and basaltic andesites ranges from 3 to 5 wt%. (Arcos et al., 1988; Polanco et al., 2015). As expected for a porphyritic lava composed by calcic plagioclase, clino and orthopyroxene, and minor olivine and magnetite as phenocrysts, K_2O content must be mostly concentrated in the glassy intersertal to hyalopilitic groundmass. However, plagioclase phenocrysts (with an average composition of $Ab_{52}An_{44}Or_3$) could also favoured the locally formation of illite during albitization of plagioclase. At the shallow zone of the drillhole (e.g. samples 262 and 281), the fluid T (T ≤ 85 °C) is only able to hydrate and dissolve the volcanic glass. This dissolution produces the release of low amounts of K, Ca, and Na and promotes the crystallization of smectite phases (or R0 I-S). With depth, the fluid T increases, becoming more reactive and more effective in dissolving most of the glass and partially plagioclase phenocrysts. Altered glass supplies enough K to the fluid to crystallize illite. Simultaneously, the increase in T also promotes the local albitization of plagioclases, releasing even more K to the system. Experimental works by Hövelmann et al. (2010) have shown that the albitization of Ca-rich plagioclase is the result of an interface-coupled dissolution-reprecipitation mechanism. Furthermore, the decrease in molar volume during the transformation of Ca-rich plagioclase to albite is only about 1%, with this albitization process consequently playing only a minor role in the generation of secondary porosity. Consequently, as shown by Hövelmann et al. (2010), secondary porosity during albitization must be predominantly controlled by the solubility differences of Ca-rich plagioclase and albite with respect to the fluid. In accordance with the conclusions of these authors, because the amount of dissolving Ca-rich plagioclase exceeds the amount of reprecipitating albite, secondary porosity would be improved during albitization. Consequently, increased albitization enhances the availability of K from primary Ca-rich plagioclase. Under these conditions, the concomitant increase in T, the dissolution of K-rich glassy material and the locally enhancement of the fluid/rock interaction as a consequence of secondary porosity and K availability (both from glass alteration and plagioclase albitization) are the main factors favouring the crystallization of K-rich clays. Thus, at T ≥ 85 °C, the conditions are appropriate for the crystallization of R1 I-S (with minor smectite + R0 I-S). R1 I-S is a relatively stable phase up to T close to 170 °C. Finally, illite crystallizes at T ≥ 175 °C, being the most abundant and stable phase at these temperatures.

In sample 282 (T = 85 °C), the transition from smectite to R1 I-S starts, and R1 I-S coexists with smectite in the matrix and with illite in fragments. This heterogeneity in the clay distribution probably indicate that the characteristics of the precursor phases condition the replacement process at very low temperature environments. The development of different microsites in the rock (matrix and fragments) may be a consequence of the diverse composition and/or particle size of the precursor materials. These textures are an evidence of the lack of equilibrium at the sample scale.

5.4. Geothermal implications

The transition from smectite to illite in geothermal systems happens in the domain of argillic alteration, conforming the so-called clay cap underlying the geothermal reservoir domain, characterized by a propyllitic alteration. Numerous researchers have shown the importance of this clay cap in the exploration stage of geothermal fields (e.g. Johnston et al., 1992, between many others). Moreover, Ferrage et al. (2011) have remarked on the importance of this illitization process to understand the thermal history of rocks in active and fossil geothermal fields. The possibility to study alteration samples from drill cores recovered in active geothermal systems is a unique opportunity to contrast in-situ measured drillholes with estimates based on mineralogical studies. Factors such as T, lithology, fluid/rock ratio, and fluid geochemistry mainly control (together with time) the intensity and nature of the alteration. Consequently, the smectite-to-illite transition is not only controlled by T, but also by kinetics. TEM images have shown differences in clays where they formed from glass replacement, plagioclase overgrowth, or directly precipitated in open spaces as pore filling.

Inoue et al. (2004, 2005) focussed the illitization sequence analysing felsic volcaniclastic rocks from drill core samples of the Kakkonda (Japan) geothermal system. The main conclusions observed by these authors in terms of the kinetic control on the smectite illitization seems to be applicable to the Tinguiririca geothermal system, where the illitization sequence has been studied in a more basic system (andesites to basaltic andesites). In general terms, as evidenced with our results, the illitization sequence observed is concordant with depth and measured drillhole T. Nevertheless, the presence of phases out of equilibrium suggests that the macroscopic interpretation of drillcore

samples, or even non-detailed XRD studies, must be considered only as a first-order estimation for T in the geothermal system.

6. Conclusions

The illitization process in the Tinguiririca geothermal field (central Chile) has been studied using different methodologies. The XRD approach suggests a continuous evolution from smectite to illite throughout the I-S R0–I-S R1–I-S R3 transition, with an increase in the illite layer percentage with depth (and T). Under TEM, a similar illitization trend has been observed, with the clays being more heterogeneous than the XRD patterns display, showing the coexistence of different types of dioctahedral clays in the same sample. Our results suggest consequently that the smectite-to-illite sequence is not as continuous as XRD seems to indicate.

Concerning the crystallization mechanism, the textures observed both by SEM and TEM indicate that clays crystallize from a fluid following the dissolution of K-rich vitreous phases and also as overgrowths of primary plagioclase. T and fluid composition favour the dissolution of the vitreous materials, which are more unstable than the crystalline components.

Finally, with respect to the different factors controlling the smectite-to-illite transition, illitization depends on the T and composition of the fluid, the fluid/rock ratio, and the composition of the precursor materials. These factors must be considered at the local scale due to the lack of equilibrium at the sample level. However, two critical factors seem to be the first-order controls in this illitization sequence: T availability and K availability deriving mainly from glass dissolution and, locally, from Ca-rich plagioclase albitization.

Acknowledgements

The authors are grateful to two anonymous reviewers for their useful suggestions. This research has been supported by Chilean Research Projects Fondecyt-Regular-1140629 and Fondap-Conicyt-15090013 Andean Geothermal Center of Excellence (CEGA), by the Spanish Ministerio de Educación y Ciencia (CGL2011-30153-C02-01, CGL2011-24101; CGL2011-29920; CGL2011-23770 and CGL2013-46169-C2-1-P), PAIDI-group RNM-179, RNM-148, and the Aragón Regional Government and the European Social Fund (Grupos Consolidados) (Grant number: E45). The authors thank the Energía Andina company (EASA) and, especially, Richard Suttill for helping provide us with access to the Pte-1 borehole samples. We also thank C. Gallego, M.A. Laguna (SAI, University of Zaragoza), and M.M. Abad (CIC, University of Granada) for her help with the electron microscopy work.

Appendix A. Supplementary data

Supplementary data to this article can be found online at http://dx.doi.org/10.1016/j.clay.2016.04.011.

References

Ahn, J.H., Peacor, D.R., 1986. Transmission electron microscope data for rectorite: implications for the origin and structure of fundamental particles. Clays Clay Miner. 34, 165–179.

Altaner, S.P., Ylagan, R.F., 1997. Comparison of structural models of mixed-layer illite/smectite and reaction mechanisms of smectite illitization. Clays Clay Miner. 45, 517–533.

Amouric, M., Olives, J., 1991. Illitization of smectite as seen by HRTEM. Eur. J. Mineral. 3, 831–835.

Arcos, R., Charrier, R., Munizaga, F., 1988. Volcanitas cuaternarias en la hoya superior del Río Tinguirrica (34°40′ L.S. – 70°21′ L.W.): características geológicas, antecedentes geoquímicos y geocronológicos. V Congreso Geológico Chileno vol. III, pp. 245–260.

Arostegui, J., Sanguesa, F.J., Nieto, F., Uriarte, J.A., 2006. Thermal models and clay diagenesis in the Tertiary-Cretaceous sediments of the Alava block (Basque-Cantabrian basin, Spain). Clay Miner. 41, 791–809.

Baronnet, A., 1992. Polytypism and stacking disorder. In: Buseck, P.R. (Ed.), Minerals and Reactions at the Atomic Scale: Transmission Electron MicroscopyReviews in Mineralogy 27. Mineralogical Society of America, pp. 231–288.

Bauluz, B., Peacor, D.R., González-López, J.M., 2000. Transmission electron microscopy study of illitization in pelites from the Iberian Range, Spain: layer-by-layer replacement? Clays Clay Miner. 48, 374–384.

Bauluz, B., Peacor, D.R., Ylagan, R.F., 2002. Transmission electron microscopy study of smectite illitization during hydrothermal alteration of a rhyolitic hyaloclastite from Ponza, Italy. Clays Clay Miner. 50, 157–173.

Beaufort, F., Rigualt, C., Billon, S., Billault, V., Inoue, A., Inoue, S., Patrier, P., 2015. Chlorite and chloritization processes through mixed-layer mineral series in low-temperature geological systems – a review. Clay Miner. 50, 497–523.

Bell, T.E., 1986. Microstructure in mixed-layer illite/smectite and its relationship to the reaction of smectite to illite. Clays Clay Miner. 34, 146–154.

Clavero, J., Pineda, G., Mayorga, C., Giavelli, A., Aguirre, I., Simmons, S., Martini, S., Soffia, J., Arriaza, R., Polanco, E., Achurra, L., 2011. Geological, geochemical, geophysical and first drilling data from Tinguiririca Geothermal Area, Central Chile. Geotherm. Resour. Counc. Trans. 35, 731–734.

Cuadros, J., Altaner, S.P., 1998a. Characterization of mixed-layer illite-smectite from bentonites using microscopic, chemical, and X-ray methods: constraints on the smectite-to-illite transformation mechanism. Am. Mineral. 83, 762–774.

Cuadros, J., Altaner, S.P., 1998b. Compositional and structural features of the octahedral sheet in mixed-layer illite/smectite from bentonites. Eur. J. Mineral. 10, 111–124.

Deng, X., Underwood, M.B., 2001. Abundance of smectite and the location of a plate-bounday fault, Barbados accretion prism. Geol. Soc. Am. Bull. 113, 495–507.

Dong, H., Peacor, D.R., Freed, R.L., 1997. Phase relations among smectite, R1 illite-smectite, and illite. Am. Mineral. 82, 379–391.

Drits, V., Lindgreen, H., Sahkarov, B.A., Salyn, A.S., 1997. Sequential structure transformation of illite-smectite-vermiculite during diagenesis of Upper Jurassic shales from the North Sea and Denmark. Clay Miner. 32, 351–371.

Droguett, B., Morata, D., Clavero, J., Pineda, G., Morales, S., Carrillo, F.J., 2012. Mineralogía de alteración en el pozo Pte-1, campo geotermal Tinguiririca, Chile. Congreso Geologico Chile-2012, pp. 500–502.

Dubacq, B., Vidal, O., De Andrade, V., 2010. Dehydratation of dioctahedral aluminious phyllosilicates: thermodynamic modelling and implications for thermobarometric estimates. Contrib. Mineral. Petrol. 15, 159–174.

Eberl, D., Srodon, J., 1988. Ostwald ripening and interparticle diffraction effects for illite crystals. Am. Mineral. 73, 1335–1345.

Essene, E.J., Peacor, D.R., 1995. Clay mineral thermometry. A critical perspective. Clays Clay Miner. 43, 540–553.

Ferrage, E., Vidal, O., Mosser-Ruck, R., Cathelineau, M., Cuadros, J., 2011. Reinvestigation of smectite illitization in experimental hydrothermal conditions: results from X-ray diffraction and transmission electron microscopy. Am. Mineral. 96, 207–223.

Guthrie, G.D., Veblen, D.R., 1989a. High-resolution transmission electron microscopy of mixed-layer illite/smectite: computer simulation. Clays Clay Miner. 37, 1–11.

Guthrie, G.D., Veblen, D.R., 1989b. High-resolution transmission electron microscopy applied to clay minerals. In: Coyne, L.M., McKeever, S.W.S., Blake, D.F. (Eds.), Spectroscopic Characterization of Minerals and their SurfacesSymposia Series 415. American Chemical Society, Washington.

Guthrie, G.D., Veblen, D.R., 1990. High-resolution transmission electron microscopy of mixed-layer illite/smectite: computer simulations. Am. Mineral. 75, 276–288.

Harvey, C.C., Browne, P.R.L., 1991. Mixed-layer clay geothermometry in the Wairakei geothermal field, New Zealand. Clays Clay Miner. 39, 614–621.

Hövelmann, J., Putnis, A., Geiser, T., Schmidt, B.C., Golla-Schindler, U., 2010. The replacement of plagioclase feldspars by albite: observations from hydrothermal experiments. Contrib. Mineral. Petrol. 159, 43–59.

Hower, J., Eslinger, E.V., Hower, M.E., Perry, E.A., 1976. Mechanism of burial metamorphism of argillaceous sediment: 1. Mineralogical and chemical evidence. Geol. Soc. Am. Bull. 87, 725–737.

Inoue, A., Kohyama, N., Kitagawa, R., Watanabe, T., 1987. Chemical and morphological evidence for the conversion of smectite to illite. Clays Clay Miner. 35, 111–120.

Inoue, A., Watanabe, T., Kohyama, N., Brusewitz, A.M., 1990. Characterization illitization of smectite in bentonite beds at Kinnekulle, Sweden. Clays Clay Miner. 34, 241–249.

Inoue, A., Meunier, A., Beaufort, D., 2004. Illite-smectite mixed-layer minerals in felsic voclaniclastic rocks from drill cores, Kakkonda, Japan. Clays Clay Miner. 52, 66–84.

Inoue, A., Lanson, B., Marques-Fernandes, M., Sakharov, B.A., Murakami, T., Meunier, A., Beaufort, D., 2005. Illite-smectite mixed-layer minerals in the hydrothermal alteration of volcanic rocks: I. One-dimensional XRD structure analysis and characterization of component layers. Clays Clay Miner. 53, 423–439.

Jagodzinski, H., 1949. Eindimensionale fehlordnung in hristallen und ihr einfluss auf die Rontgeninterferenzen. I. Berechnung des fehlordnungsgrades au der Rontgenintensitaten. Acta Crystallogr. 2, 201–207.

Ji, J., Browne, P.R.L., 2000. Relationship between illite crystallinity and temperature in active geothermal systems of New Zealand. Clays Clay Miner. 48, 139–144.

Jiang, W.T., Peacor, D.R., Merriman, R.J., Roberts, B., 1990. Transmission and electron microscopic study of mixed-layer illite/smectite formed as an apparent replacement product of diagenetic illite. Clays Clay Miner. 38, 449–468.

Johnston, J.M., Pellerin, L., Hohmann, G.W., 1992. Evaluation of electromagnetic methods for geothermal reservoir detection. Geotherm. Resour. Counc. Trans. 16, 241–245.

Kim, J.W., Peacor, D.R., Tessier, D., Elsass, F., 1995. A technique for maintaining texture and permanent expansion of smectite interlayers for TEM observations. Clays Clay Miner. 43, 51–57.

Lahsen, A., Rojas, J., Morata, D., Aravena, D., 2015. Geothermal exploration in Chile: country update. Proceeding World Geothermal Congress 2015, Melbourne, Australia, 19–25 April 2015.

Lindgreen, H., Garnæs, J., Hansen, P.L., Besenbacher, F., Lægsgaard, E., Stensgaard, I., Gould, S.A.C., Hansma, P.K., 1991. Ultrafine particles of North Sea illite/smectite clay minerals investigated by STM and AFM. Am. Mineral. 76, 1218–1222.

Lippmann, E., 1982. The thermodynamic status of clay minerals. In: Van Olphen, H., Veniale, F. (Eds.), Proceeding of the 7th International Clay Conference, Bologna, Pavia, 1981. Elsevier, New York, pp. 475–485.

Mas, A., Guisseau, D., Patrier Mas, P., Beaufort, D., Genter, A., Sanjuan, B., Girard, J.P., 2006. Clay minerals related to the hydrothermal activity of the Bouillante geothermal field (Guadeloupe). J. Volcanol. Geotherm. Res. 158, 380–400.

Moore, D.M., Reynolds, R.C., 1997. X-ray diffraction and the identification and analysis of clay minerals. Oxford University Press, Oxford (378 pp.).

Morse, J.W., Casey, W.H., 1988. Ostwald processes and mineral paragenesis in sediments. Am. J. Sci. 288, 537–560.

Murakami, T., Inoue, A., Lanson, B., Meunier, A., Beaufort, D., 2005. Illite-smectite mixed-layer minerals in the hydrothermal alteration of volcanic rocks: II. One-dimensional HRTEM structure images and formation mechanisms. Clays Clay Miner. 53, 440–451.

Nadeau, P.H., Wilson, M.J., McHardy, W.J., Tait, J.M., 1984. Interstratified clays as fundamental particles. Science 255, 923–925.

Nadeau, P.H., Wilson, M.J., McHardy, W.J., Tait, J.M., 1985. The conversion of smectite to illite during diagenesis: evidence from some illitic clays from bentonites and sandstones. Mineral. Mag. 49, 393–400.

Pavez, C., Tapia, F., Comte, D., Gutiérrez, F., Lira, E., Charrier, R., Benavente, O., 2016. Characterization of the hydrothermal system of the Tinguiririca Volcanic Complex, Central Chile, using structural geology and passive seismic tomography. J. Volcanol. Geotherm. Res. 310, 107–117.

Perry Jr., E.A., Hower, J., 1970. Burial diagenesis in Gulf Coast pelitic sediments. Clays Clay Miner. 18, 165–177.

Perry Jr., E.A., Hower, J., 1972. Late-stage dehydration in deeply buried pelitic sediments. Am. Assoc. Pet. Geol. Bull. 56, 2013–2021.

Petschick, R., 2000. MacDiff. http://www.ccp14.ac.uk/ccp/ccp14/ftp-mirror/krumm/Software/macintosh/macdiff/MacDiff.html (Accessed 18 July 2008).

Polanco, E., Pineda, G., Droguett, B., Clavero, J., Arcos, R., Pérez de Arce, C., Parra, J., 2015. Geología y geoquímica del Complejo Volcánico Tinguiririca (Pleistoceno Superior-Holoceno), Andes del Sur, Chile. XIV Congreso Geológico Chileno.

Reyes, A., 1990. Petrology of Philippine geothermal systems and the application of alteration mineralogy to their assessment. J. Volcanol. Geotherm. Res. 43, 279–309.

Tillick, D., Peacor, D.R., Mauk, J., 2001. Genesis of dioctahedral phyllosilicates during hydrothermal alteration of volcanic rocks: I. The Golden Cross epithermal ore deposit, New Zealand. Clays Clay Miner. 49, 126–140.

Vázquez, M., Nieto, F., Morata, D., Droguett, B., Carrillo-Rosua, F.J., Morales, S., 2014. Evolution of clay mineral assemblages in the Tinguiririca geothermal field, Andean Cordillera of Central Chile: an XRD and HRTEM-AEM study. J. Volcanol. Geotherm. Res. 282, 43–59.

Veblen, D.R., Guthrie Jr., G.D., Livi, K.J.T., Reynolds Jr., R.C., 1990. High-resolution transmission electron microscopy and electron diffraction of mixed-layer illite/smectite: experimental results. Clays Clay Miner. 38, 113.

Weaver, C.E., 1960. Possible uses of clay minerals in search for oil. AAPG Bull. 44, 1505–1518.

Whitney, D.L., Evans, B.W., 2010. Abbreviations for names of rock-forming minerals. Am. Mineral. 95 (1), 185–187.

Yan, Y., Tillick, D., Peacor, D.R., Simmons, S.F., 2001. Genesis of dioctahedral phyllosilicates during hydrothermal alteration of volcanic rocks: II. The Broadlannds-Ohaaki hydrothermal system, New Zealand. Clays Clay Miner. 49, 141–155.

Yau, L., Peacor, D.R., McDowell, S.D., 1987. Smectite to illite reactions in Salton Sea shales: a transmission and analytical electron microscopy study. J. Sediment. Petrol. 57, 335–342.